Communications to SIMAI Congress,
ISSN 1827-9015, Vol. 3 (2009) 237 (12pp)
DOI: 10.1685/CSC09237

A numerical code for the simulation of magma-rocks dynamics

Antonella Longo[1], Michele Barsanti[2], Paolo Papale[1], Melissa Vassalli[1], Chiara P. Montagna[1], Luca Bisconti[1], Gilberto Saccorotti[1]

[1] *Istituto Nazionale di Geofisica e Vulcanologia, sezione di Pisa*
Via U. della Faggiola 32, I-56127, Pisa, Italy
longo@pi.ingv.it
papale@pi.ingv.it
vassalli@pi.ingv.it
montagna@pi.ingv.it
bisconti@pi.ingv.it
saccorotti@pi.ingv.it

[2] *Dipartimento di Matematica Applicata "U. Dini",*
Università degli Studi di Pisa, Via F. Buonarroti 1/c, I-56127, Pisa, Italy
m.barsanti@dma.unipi.it

Abstract

We present a numerical code for the simulation of the dynamics of compressible to incompressible, multicomponent flows, based on the finite element algorithm by Hauke & Hughes (1998). Balance equations for mass, momentum, energy and composition are solved with space-time Galerkin least-squares and discontinuity-capturing stabilizing techniques. The code is used to study the dynamics of convection and mixing in magmatic systems such as replenishment of magma chambers and volcanic conduits, and it reveals the occurrence of previously not described processes. We also present the theoretical framework for the implementation of fluid-structure interaction of fully coupled magma-rock dynamics based on the deforming-spatial-domain method by Tezduyar (2006), that intrinsically includes moving meshes.

Keywords: `space-time finite element, fluid-structure interaction, magma, rock, Navier-Stokes equations, two-fields formulation.`

1. Introduction

The geophysical problem considered in this work is the fluid-structure (FS) interaction between magma in a magmatic reservoir and the surrounding rocks. The motivation is to understand the links between ground displacement data and deep volcanic processes, which are crucial for the assessment of short-term volcanic hazard (Fig. 1). The FS interaction model is based on the space-time (ST) finite-element (FE) method, by using the special deforming-spatial-domain technique (Tezduyar et al. [20]) for mov-

Received 04/02/2009, in final form 28/06/2009
Published 31/07/2009

ing meshes. The method is suitable for the simulation of non-linear and complex physical systems. The fluid formulation is stabilized with the least squares and the discontinuity capturing terms (Hauke & Hughes [7]; Shakib et al. [19]). While the fluid model has already been implemented, the solid and interface models are still under development.

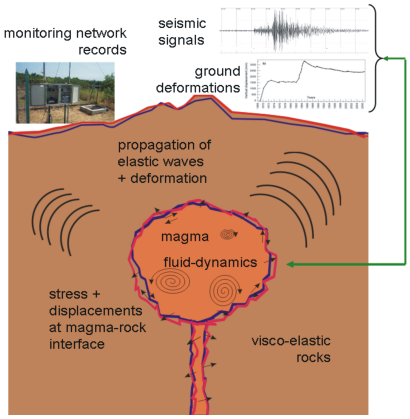

Fig. 1. Magma-rocks interaction and monitoring network.

2. Physical Model and Governing Equations

The fluid dynamics model (Longo et al. [6], [5]) consists of a single fluid (magma in applications to volcanological cases) compressible-incompressible multicomponent mixture. The components can be in liquid or gaseous state: magma is a multiphase homogeneous mixture of silicate liquid and gas bubbles. The governing equations are the mass conservation for each component, the momentum and energy balance of the mixture (Bird [1]; Lamb [2]; Landau & Lifsits [3]):

$$
\begin{aligned}
&\frac{\partial \rho y_k}{\partial t} + \nabla \cdot (\rho \mathbf{v} y_k) = -\nabla(\rho \mathcal{D}_k \Delta y_k) \quad \text{for } k = 1, \ldots, n, \\
&\frac{\partial \rho \mathbf{v}}{\partial t} + \nabla \cdot (\rho \mathbf{v} \otimes \mathbf{v} + p\mathbf{I}) = \nabla \cdot \big(\mu\big((\nabla \mathbf{v} + \mathbf{v}^T) - \frac{2}{3}(\nabla \cdot \mathbf{v})\mathbf{I}\big)\big) + \rho \mathbf{b}, \\
&\frac{\partial \rho e}{\partial t} + \nabla \cdot (\rho \mathbf{v} e + p\mathbf{v}) = \nabla \cdot \big(\mu(\nabla \mathbf{v} + \nabla \mathbf{v}^T)\mathbf{v} + \kappa \nabla T\big) + \rho(\mathbf{b} \cdot \mathbf{v} + r),
\end{aligned}
\tag{1}
$$

where $\mathbf{y} = (y_1, y_2, ..., y_n)$ are the weight fractions of components, p is pressure, κ is the thermal diffusion coefficient, T is the temperature, r is the heat supply per unit mass, e is total energy, μ is the viscosity, $\mathbf{b} = (b_1, b_2)^T$ is the body force per unit mass and $\mathcal{D}_k$ is the diffusion coefficient of component y_k. The physico-chemical properties of the magma $(\rho, \mu, c_V, \kappa, \ldots)$

DOI: 10.1685/CSC09237

depend on the local conditions of pressure, temperature, composition, velocity and phase distribution under the assumption of linear mixture (Modell & Reid [15]):

$$\begin{aligned} \frac{1}{\rho} &= \sum_{k,\,\pi} \frac{y_k^\pi}{\rho_k^\pi}, \\ e &= \sum_{k,\,\pi} y_k^\pi e_k^\pi \ \text{ with } \ e_k^\pi = c_{V,k}^\pi T, \\ \mu &= exp\Big(\sum_{k,\pi} y_k^\pi ln(\mu_k^\pi(T)) \Big), \end{aligned} \tag{2}$$

where k and π represent the indeces of components and phases, respectively. Thus, $\mu_k^\pi, \rho_k^\pi, c_{V,k}^\pi$ are viscosity, density and specific heat coefficients at constant volume of component k in phase π (Prausnitz et al. [18]). In case of magmatic mixtures, the exsolution law is computed as in Papale et al. [14]. The structural mechanics model assumes an isotropic solid material with heterogeneous density and elastic properties (i.e., Lamé coefficients μ_s and λ_s). The two dimensional linear dynamic problem is governed by the classical Newton's law for momentum conservation:

$$\frac{\partial^2 \rho \mathbf{u}}{\partial t^2} = \nabla \cdot \boldsymbol{\sigma}_{solid}(\nabla \mathbf{u}) + \rho \mathbf{g}, \ \text{ with } (\sigma_{solid})_{ik} = D_{ij}\epsilon_{jk}, \tag{3}$$

where $\boldsymbol{\sigma}_{solid}$ is the stress tensor, $\mathbf{D}$ is the elastic moduli tensor and $\boldsymbol{\epsilon}$ is the strain tensor. The fluid-structure interface model for the dynamic coupling between fluid and solid is based on continuity of displacement vectors and stress tensors at the interface (with no-slip fluid boundary conditions at the chamber walls) (Michler et al. [13]):

$$\begin{cases} \mathbf{v}_{fluid} = \mathbf{v}_{solid}, \\ \boldsymbol{\sigma}_{fluid} + p\mathbf{I} = \boldsymbol{\sigma}_{solid}. \end{cases} \tag{4}$$

where $\mathbf{v}_{solid} = \partial \mathbf{u}/\partial t$.

2.1. *Governing Equations in Compact Form*

In compact notation, equations (1) are rewritten as:

$$\frac{\partial \mathbf{U}}{\partial t} + div_{\mathbf{x}}(\mathbf{F}) - \mathfrak{J} = \mathbf{0}. \tag{5}$$

where $\mathbf{F} = \mathbf{F}^{adv} - \mathbf{F}^{diff}$ and

$$
\begin{aligned}
&\mathbf{U} = \rho(\mathbf{y}, v_1, v_2, e)^T, \\
&\mathbf{F}_i^{adv} = \rho v_i(\mathbf{y}, v_1, v_2, e)^T + p(\mathbf{0}, \delta_{1i}, \delta_{2i}, v_i)^T, \\
&\mathbf{F}_i^{diff} = (\mathbf{0}, \tau_{1i}, \tau_{2i}, \tau_{ij}v_j)^T + (-\mathbf{J}_i, 0, 0, -q_i - \sum_{k=1}^{n} J_i^k h_k)^T, \\
&\mathfrak{J} = (\mathbf{0}, b_1, b_2, b_j v_j + r)^T,
\end{aligned}
\tag{6}
$$

$q_i = \kappa T_{,i}$ are the components of the heat-flux, $\tau_{ij} = \mu\big((u_{i,j}+u_{j,i}) - \frac{2}{3}u_{k,k}\delta_{i,j}\big)$ denote the coefficients of the viscous stress tensor, J_i^k are the diffusive fluxes of mass components, h_k are the entalphy components and $\mathfrak{J}$ denotes the source vector. Defining the ST fluxes $\boldsymbol{\mathcal{F}} = [\,\boldsymbol{\mathcal{F}}_t \,|\, \boldsymbol{\mathcal{F}}_{\mathbf{x}}]$, and the ST divergence as $div_{t,\mathbf{x}} = [\,\partial/\partial t \,|\, \nabla_{\mathbf{x}}\,]$:

$$
\begin{aligned}
&\boldsymbol{\mathcal{F}}_{fluid}(\mathbf{U}) = \left[\mathbf{U} \,\middle|\, \mathbf{F}\right] \Rightarrow div_{t,\mathbf{x}}(\boldsymbol{\mathcal{F}}_{fluid}(\mathbf{U})) = \frac{\partial \mathbf{U}}{\partial t} + div_{\mathbf{x}}(\mathbf{F}), \\
&\boldsymbol{\mathcal{F}}_{solid}(\mathbf{u}) = \left[\frac{\partial \rho \mathbf{u}}{\partial t} \,\middle|\, -\mathbf{D}\boldsymbol{\epsilon}\right] \Rightarrow div_{t,\mathbf{x}}(\boldsymbol{\mathcal{F}}_{solid}(\mathbf{U})) = \frac{\partial^2 \rho \mathbf{u}}{\partial t^2} - div_{\mathbf{x}}(\mathbf{D}\boldsymbol{\epsilon}),
\end{aligned}
\tag{7}
$$

conservation equations can be further rewritten in compact notations as:

$$
div_{t,\mathbf{x}}(\boldsymbol{\mathcal{F}}) - \mathfrak{J} = 0. \tag{8}
$$

The fluid dynamics equations are solved in primitive variables $\mathbf{Y} = (y_1, y_2, ..., y_n, p, T, \mathbf{v})$ (Hauke & Hughes [7]). This formulation gives the correct behaviour in both compressible and incompressible regimes, it is robust in capturing singularities and high shocks, it provides a simple way to specify boundary conditions, and it is immediate for physical interpretation of the results. The change of variables from conservative to primitive:

$$
\overbrace{(\rho y_1,\, \ldots,\, \rho y_{n-1},\, \rho y_n,\, \rho \mathbf{v},\, \rho e_t)^T}^{\mathbf{U}=} \longrightarrow \overbrace{(y_1,\, \ldots,\, \rho y_{n-1},\, y_n,\, p,\, \mathbf{v},\, T)^T}^{\mathbf{Y}=}, \tag{9}
$$

allows to rewrite (7) as:

$$
div_{t,\mathbf{x}}(\boldsymbol{\mathcal{F}}_{fluid}(\mathbf{U}(\mathbf{Y}))) = \mathbf{U}_{,\mathbf{Y}}\mathbf{Y}_{,t} + \mathbf{F}_{,\mathbf{U}}\nabla_{\mathbf{x}}\mathbf{Y}, \tag{10}
$$

where $\mathbf{U}_{,\mathbf{Y}}$ is the Jacobian matrix for the change of variables:

$$
\mathbf{U}_{,\mathbf{Y}} = \frac{\partial(\rho y_1, \rho y_2, \ldots, \rho y_n, \rho \mathbf{v}, \rho e_t)}{\partial(y_1, y_2, ..., y_n, p, T, \mathbf{v})}, \tag{11}
$$

DOI: 10.1685/CSC09237

and $\mathbf{F}_{,\mathbf{U}}$ is similarly defined. It is useful to rewrite equation (5) in quasi-linear form:

$$\mathbf{U}_{,t} + \mathbf{A}_i \mathbf{U}_{,i} - (\mathbf{K}_{ij}\mathbf{U}_{,j})_{,i} - \mathfrak{I} = \mathbf{0}. \tag{12}$$

where $\mathbf{U}_{,i} = \partial \mathbf{U}/\partial \mathbf{x_i}$, $\mathbf{A}_i = \mathbf{F}^{adv}_{i,\mathbf{U}}$ is the i-th Euler-Jacobian matrix, and $\mathbf{K} = (\mathbf{K}_{ij})$ is the diffusivity matrix satisfying the relation $\mathbf{K}_{ij}\mathbf{U}_{,j} = \mathbf{F}^{diff}_i$. The quasi-linear form with respect to the primitive variables $\mathbf{Y}$ is:

$$\mathbf{U}_{,\mathbf{Y}}\mathbf{Y}_{,t} + \mathbf{A}_i(\mathbf{U}_{,\mathbf{Y}})_{ij}\mathbf{Y}_{,j} - (\mathbf{K}_{ij}(\mathbf{U}_{,\mathbf{Y}})_{jk}\mathbf{Y}_{,k})_{,i} + \mathbf{S}\mathbf{Y} = \mathbf{0}, \tag{13}$$

where $\mathfrak{I} = -\mathbf{S}\mathbf{Y}$ and $\mathbf{S}$ is the source matrix.

3. Mesh Model

The mesh deformation is governed by the equation of elasticity, with pseudo-Lamé coefficients that depend on the shape of the mesh, in order to avoid excessive distortion (Tezduyar et al. [20]). The FS interface and the Earth surface have to follow the material motion of the fluid and/or rock. Hence, the movement of internal mesh nodes is determined imposing node velocities equal to fluid and/or rock velocities at FS interface and at Earth surface.

4. Space-Time Finite Element Formulation

The ST finite element formulation uses weighting and trial functions dependent on space and time. The whole computational domain Q is given by the evolution in time of the space domain from the initial to the final configuration (Fig. 2): it is subdivided into ST slabs Q_n, representing the evolution between times t_n and t_{n+1} of the space domain (Fig. 3). The T-discontinuous/S-continuous method adopts weighting and trial functions that are continuous in space and discontinuous in time. In this manner, the weak formulation integrates over successive ST slabs Q_n, assigning causal time boundary conditions on the solution between consecutive slabs (Fig. 3).

Considering the ST compact notation (8), the ST weak formulation over a time slab is:

$$\int_{Q_n} \mathbf{W}(\mathbf{x},t) \cdot div_{t,\mathbf{x}}(\boldsymbol{\mathcal{F}}^{flux}) dQ + \int_{\Omega_{n-1}} \mathbf{W}(\mathbf{x},t_n^+)(\mathbf{U}(t_n^+) - \mathbf{U}(t_n^-)) d\Omega + \text{stabilizing terms} = 0. \tag{14}$$

where $\boldsymbol{\mathcal{F}}^{flux}$ may equal $\boldsymbol{\mathcal{F}}_{fluid}$ or $\boldsymbol{\mathcal{F}}_{solid}$. The ST formulation naturally includes the mesh deformation: it is equivalent to the ALE formulation

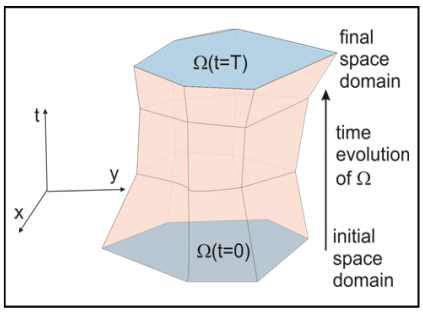

Fig. 2. The space-time domain Q.

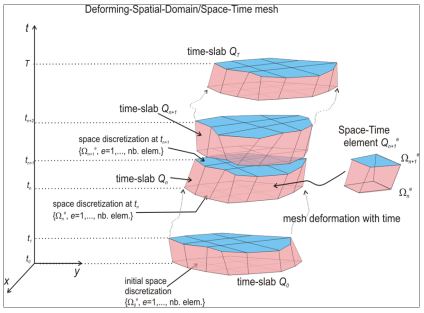

Fig. 3. Space-time slabs Q_n.

as it results from integration by parts in space and time of equation (14) (Masud & Hughes [12]; van der Vegt & van der Ven [21]). Integrating by parts and applying the Gauss theorem to the first term in (14) it follows:

$$
\begin{aligned}
&\int_{Q_n} \mathbf{W}(\mathbf{x},t)\cdot div_{t,\mathbf{x}}(\boldsymbol{\mathcal{F}}^{flux})dQ = -\int_{Q_n} grad_{t,\mathbf{x}}(\mathbf{W})^T : \boldsymbol{\mathcal{F}}^{flux} dQ \\
&+\int_{P_n} \mathbf{n}_s\cdot\big(\mathbf{W}^T\boldsymbol{\mathcal{F}}^{flux}_{\mathbf{x}}(\mathbf{U})\big)dP + \int_{\Omega_n}\mathbf{W}^T\boldsymbol{\mathcal{F}}^{flux}_t((\mathbf{U})(t_n))d\Omega \\
&-\int_{\Omega_{n-1}}\mathbf{W}^T\boldsymbol{\mathcal{F}}^{flux}_t(\mathbf{U}(t_{n-1}))d\Omega,
\end{aligned}
\tag{15}
$$

where $\mathbf{n}_{st} = (\mathbf{n}_s,\, \mathbf{n}_t)$ is the unit outward normal vector at the ST boundary $\partial Q_n = \Omega_{n-1}\cup\Omega_n\cup P_n$. Here, Ω_{n-1} and Ω_n are the space flow domain $\Omega(t)$ levels at the time steps t_{n-1}, t_n respectively, and P_n is the lateral slab boundary. Applying (15) for the fluid equations, the ST weak form reads:

$$
\begin{aligned}
&\text{find } \mathbf{U}\in\mathcal{V}_n \text{ such that } \forall\ \mathbf{W}\in\mathcal{W}_n : \\
&\overbrace{\int_{Q_n}\big(-\mathbf{W}_{,t}\cdot\mathbf{U}(\mathbf{Y}) - \mathbf{W}_{,i}\cdot\mathbf{F}_i(\mathbf{Y}) - \mathbf{W}\cdot\mathfrak{J}\big)dQ}^{\text{(weak NS equations)}} \\
&+\overbrace{\int_{\Omega_{n-1}}\big(\mathbf{W}(t_{n+1}^-)\cdot\mathbf{U}(\mathbf{Y}(t_{n+1}^-)) - \mathbf{W}(t_n^+)\cdot\mathbf{U}(\mathbf{Y}(t_n^-))\big)d\Omega}^{\text{(Jump-condition + time-boundary weak NS term)}} \\
&+\sum_{e=1}^{(n_{el})_n}\int_{Q_n^e}\mathcal{L}\mathbf{W}\cdot\boldsymbol{\tau}_{\mathbf{Y}}\big(\mathcal{L}\mathbf{Y}-\mathfrak{J}\big)dQ \qquad \text{(Least-Squares)}
\end{aligned}
\tag{16}
$$

DOI: 10.1685/CSC09237

$$
\begin{aligned}
&+ \sum_{e=1}^{(n_{el})_n} \int_{Q_n^e} \nu^h(\mathbf{g}^{ij}\mathbf{W}_{,i}) \cdot \big(\mathbf{U}_{,\mathbf{Y}}\mathbf{Y}_{,j}\big) dQ \quad \text{(Discontinuity Capturing)} \\
&= \int_{P_n} \mathbf{W} \cdot \mathbf{F}_i(\mathbf{Y}) n_i dP, \qquad \text{(space-boundary weak NS term)}
\end{aligned}
$$

where $\mathcal{V}_n$ and $\mathcal{W}_n$ are the space of the trial and weighting functions respectively, $\mathcal{L} = \mathbf{U}_{,\mathbf{Y}}\partial_{,t} + \mathbf{F}^{adv}_{i,\mathbf{Y}}\partial_{,i} - (\partial_{,i})(\mathbf{K}_{ij}\partial_{,j}) + \mathbf{S}$ is the differential operator associated to the quasi-linear form of the equations (13), $\boldsymbol{\tau}_{\mathbf{Y}}$ is the matrix of intrinsic time-scales for equations in primitive variables, $(\mathbf{g}^{ij})$ is the metric tensor for the change of coordinates and ν^h is the discontinuity capturing operator. Equation (15) is used also for the solid mechanics equation (3) within the two-fields formulation (Hughes & Hulbert [9]), where both displacements $\mathbf{u}$ and velocities $\mathbf{v}$ are taken as unknowns. The complete ST weak problem is formulated as:

$$
\begin{aligned}
&\text{find } (\mathbf{u}, \mathbf{v}) \in \mathcal{V}_n \ \text{ such that } \forall\ \mathbf{W} = (\mathbf{W}_{\mathbf{u}}, \mathbf{W}_{\mathbf{v}}) \in \mathcal{W}_n : \\
&\left.\begin{aligned}
0 = &\int_{Q_n} \big(grad_{t,\mathbf{x}}(\mathbf{W}_{\mathbf{v}})^T : \boldsymbol{\mathcal{F}}_{solid} - \mathbf{W}_{\mathbf{v}} \cdot \rho\mathbf{g}\big) dQ \\
&+ \int_{\partial Q_n} \mathbf{n}_{st} \cdot \big((\mathbf{W}^-_{\mathbf{v}})^T \boldsymbol{\mathcal{F}}_{solid}(\mathbf{u}^-)\big) dS
\end{aligned}\right\} \text{(equation of motion)} \\
&+ \int_{Q_n} \nabla\mathbf{W}_{\mathbf{u}} \cdot \boldsymbol{\sigma}_{solid}(\nabla\mathbf{u})\big(\frac{\partial \mathbf{u}}{\partial t} - \mathbf{v}\big) dQ \qquad \text{(definition of velocity)} \\
&+ \int_{\Omega_{n-1}} (\nabla\mathbf{W}_{\mathbf{u}})(t_n^+) \cdot \boldsymbol{\sigma}_{solid}(\nabla\mathbf{u})[\mathbf{u}_n] d\Omega \quad \text{(displacement continuity)} \\
&+ \int_{\Omega_{n-1}} \rho\mathbf{W}_{\mathbf{v}}(t_n^+) \cdot [\mathbf{v}_n] d\Omega, \qquad \text{(velocity continuity)}
\end{aligned}
\tag{17}
$$

where $[\mathbf{u}_n] = \mathbf{u}(t_n^+) - \mathbf{u}(t_n^-)$ and $[\mathbf{v}_n]$ is defined similarly (Li & Wiberg [4]). The first two integrals constitute the T-discontinuous Galerkin formulation for the equation of motion, and the last two provide the mechanism by which the information is propagated from one ST slab to the next.

5. Solution technique

The element by element computation is performed by partitioning each space-time slab Q_n into isoparametric quadrilateral elements $\mathcal{Q}_n^e$, $e = 1, 2, \ldots, n_{el}$, (Fig. 3) bilinear in space and linear in time. Trial and weighting functions for slab Q_n, $\mathbf{V}_n^e \in \mathcal{V}_n$ and $\mathbf{W}_n^e \in \mathcal{W}_n$ are linear combinations of first-order Lagrangian polynomials in space and time, defined on the

reference element as:

$$
\begin{aligned}
\mathbf{V}_n^e(\boldsymbol{\xi},\theta) &= \sum_{a=1}^{(n_{np})_{(n)}} N_a^{(n)}(\boldsymbol{\xi})\big(\pi_{n+1}(\theta)\mathbf{V}_{a(n+1)} + \pi_n(\theta)\mathbf{V}_{a(n)}\big),\\
\mathbf{W}_n^e(\boldsymbol{\xi},\theta) &= \sum_{a=1}^{(n_{np})_{(n)}} N_a^{(n)}(\boldsymbol{\xi})\big(\pi_{n+1}(\theta)\mathbf{W}_{a(n+1)} + \pi_n(\theta)\mathbf{W}_{a(n)}\big),
\end{aligned}
\tag{18}
$$

where $(n_{np})_{(n)}$ is the number of nodal point per element, $N_a(\boldsymbol{\xi})$ are the basis functions for the quadrilateral space elements, $\pi_{n+1}(\theta) = (\theta_{n+1} - \theta)/\Delta\theta$ and $\pi_n(\theta) = (\theta - \theta_n)/\Delta\theta$ are the basis functions for the time coordinate (Tezduyar et al. [20]). Introducing finite dimensional trial and weighting function spaces $\mathcal{V}_n$ and $\mathcal{W}_n$ into (16) and (17) the following discretized equations, for fluid and solid, are obtained:

$$
\mathbf{G}\big(\mathbf{W}\,;\mathbf{V},\mathbf{V}_{n-1}\big) = 0,\ \forall\ \mathbf{W}\in\mathcal{W}_n,
\tag{19}
$$

where $\mathbf{G}$ is the operator associated to the weak problems (16) and (17), $\mathbf{V}$ is the vector of the unknowns and $\mathbf{V}_{n-1}$ is the solution on the previous slab Q_{n-1}. Since $\mathbf{G}$ is such that $\mathbf{G}\big(\mathbf{W}\,;\mathbf{V},\mathbf{V}_{n-1}\big) = \mathbf{W}\cdot\mathbf{G}(\mathbf{V},\mathbf{V}_{n-1})$, it follows the generalized principle of virtual work:

$$
\mathbf{W}\cdot\mathbf{G}(\mathbf{V},\mathbf{V}_{n-1}) = 0 \iff \mathbf{G}(\mathbf{V},\mathbf{V}_{n-1}) = \mathbf{0}\ \forall\mathbf{W}\in\mathcal{W}_n.
\tag{20}
$$

The non-linear system of equations (20), as for fluid or non-linear elasticity, can be linearized through a predictor multi-corrector Newton-Raphson method, based on first order Taylor series expansion of $\mathbf{G}$:

$$
\mathbf{G}(\mathbf{V}^{(i+1)},\mathbf{V}_{n-1}) \cong \mathbf{G}(\mathbf{V}^{(i)},\mathbf{V}_{n-1}) + \frac{\partial\mathbf{G}(\mathbf{V}^{(i)},\mathbf{V}_{n-1})}{\partial\mathbf{V}}\Delta\mathbf{V}^{(i)},
\tag{21}
$$

where $\mathbf{V}^{(i)}$ is the i-th iterative approximation of the solution $\mathbf{V}_n = (\mathbf{V}(t_{n-1}^+),\mathbf{V}(t_n^-))$ on Q_n, and $\Delta\mathbf{V}^{(i)} = \mathbf{V}^{(i+1)} - \mathbf{V}^{(i)}$. The predictor phase sets $\mathbf{V}^{(0)} = \mathbf{V}_{n-1}$, then each correction pass computes the i-th iterative $\mathbf{V}^{(i)}$. Imposing that:

$$
\begin{aligned}
&\mathbf{G}(\mathbf{V}^{(i)},\mathbf{V}_{n-1}) + \frac{\partial\mathbf{G}(\mathbf{V}^{(i)},\mathbf{V}_{n-1})}{\partial\mathbf{V}}\Delta\mathbf{V}^{(i)} = \mathbf{0} \iff\\
&\underbrace{\frac{\partial\mathbf{G}(\mathbf{V}^{(i)},\mathbf{V}_{n-1})}{\partial\mathbf{V}}}_{=\mathbf{M}^{(i)}}\Delta\mathbf{V}^{(i)} = \underbrace{-\mathbf{G}(\mathbf{V}^{(i)},\mathbf{V}_{n-1})}_{=\mathbf{R}^{(i)}},
\end{aligned}
\tag{22}
$$

the following linearized problem is obtained:

$$
\mathbf{M}^{(i)}\Delta\mathbf{V}^{(i)} = \mathbf{R}^{(i)},
\tag{23}
$$

DOI: 10.1685/CSC09237

where $\mathbf{M}^{(i)}$ is the tangent matrix and $\mathbf{R}^{(i)}$ the residual vector. For each iterative step the system (23) is numerically solved and $\mathbf{V}^{(i+1)} = \Delta\mathbf{V}^{(i)} + \mathbf{V}^{(i)}$ is retrieved. When the residual vanishes below convergence threshold, the obtained value $\mathbf{V}^{(i_{max})}$ gives the required approximation of $\mathbf{V}_n$ (Shakib et al. [19]). Element by element contributions are computed with 2 point Gauss integration, and system (23) is solved with a diagonal block-preconditioned GMRES. In the case of linear elasticity direct solution is performed.

6. Code engineering

The numerical algorithm is implemented as a C++ software. Object Oriented and Template Metaprogramming rational techniques are adopted in order to decouple responsabilities and dependencies of classes, to obtain an optimized incapsulation of data, and to increase the code reusability. Furthermore, codified strategies like design patterns (e.g. observer, decorator, composite, singleton...) are widely used in order to approach commonly occurring problems in class interactions. A detailed Doxygen documentation is provided. The TRILINOS [8] parallel computational C++ library provides an efficient parallel distribution of variables and computations among processors in order to balance RAM and CPU usage and decrease interprocessors communication.

7. Numerical cases

The fluid formulation, which has already been implemented, was verified and validated with laboratory experiments, exact solutions, and numerical results taken from the literature, such as Poiseuille flow, driven cavity, 2D shock-interface interaction, broken dam (described below), Kelvin-Helmholtz instability and a some cases of gravitational instability and shock waves propagation. The considered cases span the compressible-incompressible regimes, and involve low to high viscosity fluids, with Re$\in$[0-10^6], Pr$\in$[1-7], Sc$\in$[0-10^6] and M$\in$[0-3]. CFL numbers are in the range 10^{-2}-10^4. The complete list of test cases, and detailed results can be found at http://www.pi.ingv.it/user/longo/gales/gales. Volcanological cases can be found in Longo et al. [6] and [5]. The broken dam is a test on body force contribution and advection of internal interfaces, with fluids being water and air. The examples in [17] and [16] are reproduced. The same grid spacing and time step given in [17] and [16] are also used in each example. Fig. 4 reports the contour line of 0.5 volume fraction calculated with the present model, along with the same contour lines from [16]. Fig. 5 shows the comparison between the present two simulation results and those from [17] and [16], along with the experimental data from [11]. There is a

better agreement with the results from [17] than with those from [16]. For each pair of simulations (present and [17], present and [16]) the discrepancy with the experimental results from [11] is of the same magnitude. The 2D

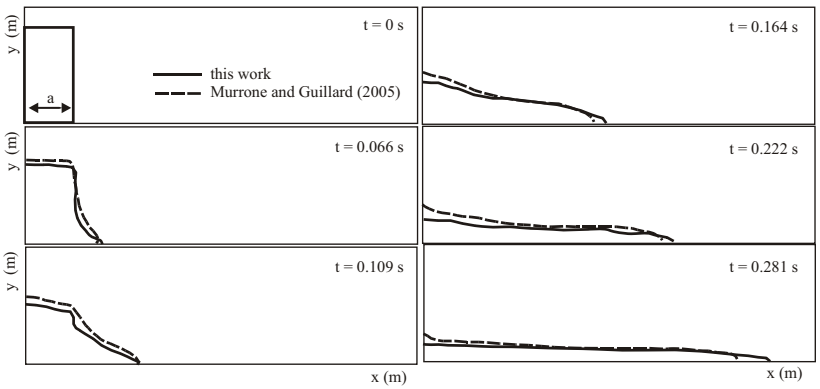

Fig. 4. Broken dam: initial conditions, and contours corresponding to 0.5 volume fraction at different times (this work: solid line; [16]: dashed line).

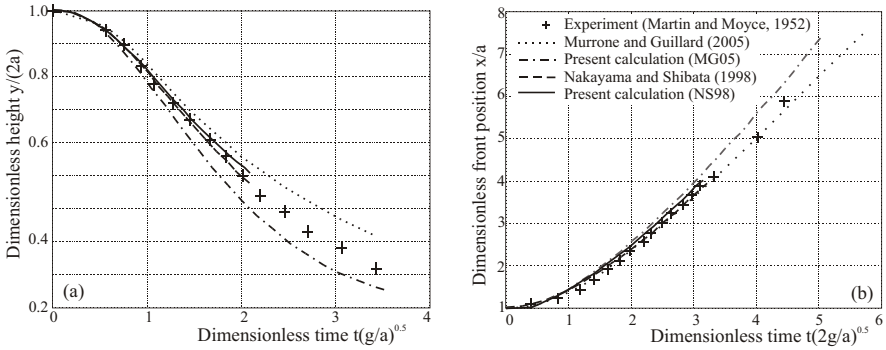

Fig. 5. (a) Dimensionless height of the column, (b) dimensionless front position. Comparison between experimental data (crosses), numerical results from [16] (dotted line, MG05), from [17] (dashed line, NS98), and present calculations. Cases MG05 and NS98 correspond to conditions similar to [16] (dash-dotted line) and [17] (solid line), respectively.

shock-interface interaction case consists in the reflection and refraction of a Mach 2 planar shock over an oblique contact discontinuity and the displacement of the interface [10]. The physical properties of inviscid perfect gases, initial and boundary conditions and time step reported in [10] are used. The computational domain is 0.5×0.6 m, discretized into 100×100 elements; the time step is $2.5\cdot10^{-6}$ s. The calculated density distribution (Fig. 6) shows that the model is able to correctly predict the positions of the reflected shock and of the compositional discontinuity. On the contrary,

DOI: 10.1685/CSC09237

the determination of the reflected shock is less accurate, approximating the uncorrected solution of [10].

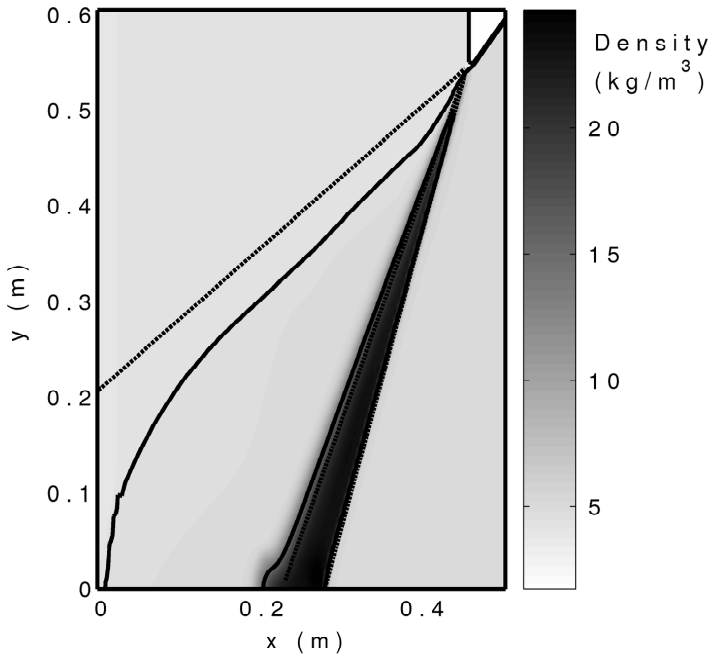

Fig. 6. 2D interaction of a shock with a contact discontinuity from [10]: density colormap and contours of 3, 4.5 and 15 kg/m^3 resulting from this work (black line) and exact solution (dashed line).

REFERENCES

1. R. B. Bird, W. E. Stewart, and E. N. Lightfoot, Fenomeni di trasporto. *Casa Ed. Ambrosiana* (1979).
2. Lamb Sir Horace, Hydrodynamics. *Cambridge University Press* (1993).
3. L. D. Landau, and E. M. Lifshits, Fluid Mechanics. *Elsevier* (1959).
4. X. D. Li, and N. E. Wiberg, Implementation and adaptivity of a space-time method for structural dynamics. *Comput. Methods Appl. Mech. Engrg.*, **156** (1998), pp. 211–229.
5. A. Longo, D. Barbato, P. Papale, G. Saccorotti, and M. Barsanti Numerical simulation of the dynamics of fluid oscillations in a gravitationally unstable, compositionally stratified fissure *Lane, S.J. Gilbert, J. S. (eds) Fluid Motions in Volcanic Conduits: A Source of Seismic and Acoustic Signals. Geological Society, London, Special Publications* **307** (2008), pp. 33–44.
6. A. Longo, M. Vassalli, P. Papale, and M. Barsanti, Numerical simulation of convection and mixing in magma chambers replenished with CO_2 -rich magma.

Geophys. Res. Lett., **33** (2006), L21305.

7. G. Hauke, and T. J. R. Hughes, A comparative study of different sets of variables solving compressible and incompressible flows. *Comput. Methods Appl. Mech. Engrg.*, **153** (1998), pp. 1–44.
8. M. Heroux et al., Sandia National Laboratories, http://trilinos.sandia.gov, The Trilinos Project, Trilinos Release 9.0 (2009).
9. T. J. R. Hughes, and G. M. Hulbert, Space-time finite element methods for elastodynamics: Formulations and error estimates. *Comput. Methods Appl. Mech. Engrg.*, **66** (1988), pp. 339–363.
10. P. Jenny, B. Müller, and H. Thomann, Correction of conservative Euler solvers for gas mixtures. *J. Comput. Phys.*, **132** (1997), pp. 91–107.
11. J. C. Martin, and W. J. Moyce, An experimental study of the collapse of liquid columns on a rigid horizontal plane, *Phil. Trans. R. Soc. Lond.*, **244** (1955), pp. 312–324.
12. A. Masud, and T. J. R. Hughes, A space-time Galerkin/least-squares finite element formulation of the Navier-Stokes equations for moving domain problems. *Comput. Methods Appl. Mech. Engrg.*, **146** (1997), pp. 91–126.
13. C. Michler, E. H. van Brummelen, S. J. Hulshoff, and R. de Borst, The relevance of conservation for stability and accuracy of numerical methods for fluid-structure iteraction. *Comput. Methods Appl. Mech. Engrg.*, **192** (2003), pp. 4195–4215.
14. P. Papale, R. Moretti, and D. Barbato, The compositional dependence of the saturation surface of $H_2O + CO_2$ fluids in silicate melts. *Chem. Geol.*, **229** (2006).
15. M. Modell, and R. C. Reid, Thermodynamics and its applications. *Prentice Hall*, (1983).
16. A. Murrone, and H. Guillard, A five equation reduced model for compressible two phase flow problems. *J. Comput. Phys.*, **202** (2005), pp. 664–698.
17. T. Nakayama, and M. Shibata, A finite element technique combined with gas-liquid two-phase flow calculation for unsteady free surface flow problems. *Computational Mechanics*, **22** (1998), pp. 194–202.
18. J. M. Prausnitz, R. N. Lichtenthaler, and E. G. de Azevedo, Molecular thermodynamics of fluid-phase equilibria. *Prentice Hall*, (1986).
19. F. Shakib, T. J. R. Hughes, and Z. Johan, A new finite element formulation for computational fluid dynamics: X. The compressible Euler and Navier-Stokes equations. *Comput. Methods Appl. Mech. Engrg.*, **89** (1991), pp. 141–219.
20. T. E. Tezduyar, S. Sathe, R. Keedy, and K. Stein, Space-time finite element techniques for computation of fluid-structure interactions. *Comput. Methods Appl. Mech. Engrg.*, **195** (2006), pp. 2002–2027.
21. J. J. W. van der Vegt, and H. van der Ven, Space-time discontinuous Galerkin finite element method with dynamic grid motion for inviscid compressible flows. *J. Comput. Phys.*, **182** (2002), pp. 546–585.